Sac1 links phosphoinositide turnover to cryptococcal virulence

Elizabeth A. Gaylord[1], Hau Lam Choy[1,2], Guohua Chen[1,3], Sydney L. Briner[1], and Tamara L. Doering[1,*]

[1]Department of Molecular Microbiology, Washington University School of Medicine, St. Louis, MO, USA

[2]Current position: L.E.K. Consulting, Boston, MA, USA

[3]Current position: Pfizer, Inc., Chesterfield, MO, USA

*Corresponding author: doering@wustl.edu

Running head: Sac1 links PI turnover to cryptococcal virulence

KEYWORDS

Cryptococcus neoformans, mycology, phosphoinositide, PI4P, phosphatase, Sac1, virulence

ABSTRACT

Cryptococcus neoformans is an environmentally-acquired fungal pathogen that causes over 140,000 deaths per year. Cryptococcal infection occurs when infectious particles are deposited into the lung, where they encounter host phagocytic cells. *C. neoformans* may be engulfed by these phagocytes, an important step of infection that leads to outcomes ranging from termination of infection to cryptococcal dissemination. To study this critical process, we screened approximately 4,700 cryptococcal gene deletion mutants for altered uptake, using primary mouse and human phagocytic cells. Among the hits of this screen, we identified 93 mutants with perturbed uptake in both systems, as well as others with differences in uptake by only one cell type. We further screened the hits for changes in thickness of the capsule, a protective polysaccharide layer around the cell which is an important cryptococcal virulence factor. This second screen yielded 131 mutants, including one lacking the phosphatidylinositol-4-phosphate phosphatase Sac1. In this work, we implicate Sac1 in both host cell uptake and capsule production. We found that *sac1* mutants exhibit lipid trafficking defects, reductions in secretory system function, and changes in capsule size and composition. Many of these changes occur specifically in tissue culture media, highlighting the role of Sac1 phosphatase activity in responding to the stress of host-like conditions. Overall, these findings show how genome-scale screening can identify cellular factors that contribute to our understanding of cryptococcal biology and demonstrate the role of Sac1 in determining fungal virulence.

IMPORTANCE

Cryptococcus neoformans is a fungal pathogen with significant impact on global health. Cryptococcal cells inhaled from the environment are deposited into the lungs, where they first contact the human immune system. The interaction between *C. neoformans* and host cells is critical because this step of infection can determine whether the fungal cells die or proliferate within the human host. Despite the importance of this stage of infection, we have limited knowledge of cryptococcal factors that influence its outcome. In this study, we identify cryptococcal genes that affect uptake by both human and mouse cells. We also identify mutants with altered capsule, a protective coating that surrounds the cells to shield them from the host immune system. Finally, we characterize the role of one gene, *SAC1*, in these processes. Overall, this study contributes to our understanding of how *C. neoformans* interacts with and protects itself from host cells.

INTRODUCTION

Cryptococcus neoformans is a fungal pathogen that causes significant mortality in immunocompromised individuals, particularly those with HIV/AIDS (1). Despite recent advances in healthcare access and treatments, cryptococcal meningitis still leads to 19% of AIDS-related deaths (2). The interaction between *C. neoformans* and host phagocytes begins when fungal cells acquired from the environment are deposited in the lung. Subsequent phagocytosis may lead to fungal cell death and termination of the infection. However, in some cases cryptococcal cells can withstand the pressures exerted by phagocytes to survive and proliferate within phagolysosomes (3–6). In this scenario, engulfment of the yeast likely enhances cryptococcal dissemination from the lung to other sites (7). Due to the importance of this initial phase of cryptococcal pathogenesis in determining how infection will progress, extensive efforts have been devoted to studying the interactions of *C. neoformans* with host phagocytic cells.

C. neoformans produces multiple factors which modulate its interactions with host cells and thereby provide protection from phagocytosis. These include the secreted peptide App1, which inhibits complement-mediated phagocytosis (8), as well as the cell wall and surrounding polysaccharide capsule. These last two are complex glycan-based structures which change in size and composition in response to environmental conditions. Strains with perturbations of the cell wall and capsule often exhibit increased uptake by phagocytic cells (9, 10), demonstrating the importance of capsule for protecting against phagocytosis.

Various models have been used to interrogate cryptococcal-host interactions. These include invertebrate and vertebrate animals, amoeba, and primary and immortalized cells (3, 11–17). Genetic screens based on libraries of mutant host or fungal cells have successfully identified gene products that modulate interactions of cryptococci with specific cell lines. In one example, Chun and colleagues subjected cryptococcal cells to insertional mutagenesis and identified mutations that affected their uptake by RAW264.7 macrophages (18). Srikanta et al. used RNA interference and high-throughput imaging to find host regulatory genes which govern the interactions of *C. neoformans* with THP-1 cells and discovered 25 fungal-specific regulators of phagocytosis (19). By applying a similar high-throughput imaging assay to a *C. neoformans* gene deletion collection (20), Santiago-Tirado et al. identified 56 fungal genes that affect uptake by THP-1 cells (10). A common strength of these studies is the genetic tractability and accessibility of the immortalized cell lines used. However, such lines lack some features of primary host cells (21–23), which may limit these approaches. Screens may also be constrained by the availability and size of *Cryptococcus* mutant collections. For example, the last study cited screened a library of

approximately 1,200 single gene deletion mutants (10), whereas much larger libraries are currently available, increasing our power to identify novel phenotypes.

This report incorporates several important departures from previous studies directed at elucidating factors important in *C. neoformans*-host interactions. First, we screened a large collection of 4,692 single gene deletion mutants, representing over eighty percent of the non-essential genes in the cryptococcal genome. Second, we applied a flexible medium-throughput imaging method that avoids pitfalls of earlier studies, such as difficulty distinguishing adherent versus internalized yeast cells (24). Third, we screened using primary cells from both mouse (murine bone marrow-derived macrophages; BMDMs) and human (monocyte derived macrophages; HMDMs), to take advantage of a model system while also examining the system of greatest clinical interest. Finally, we reasoned that many of our hits would have altered capsules, so we further tested the mutants that demonstrated altered phagocytosis for changes in capsule thickness. Overall, we identified 93 mutants that exhibit altered uptake by both murine and human phagocytes and 131 strains with alterations in capsule size (Figure 1A).

Cryptococcal capsule production is not well understood, and our knowledge of the steps of capsule secretion and surface attachment of capsule material is particularly limited (25). While it is known that capsule material traffics at least in part through the secretory pathway (26), few proteins involved in this process have been characterized. To address this gap, we focused on mutants that might be defective in the trafficking of capsular material. We became particularly interested in one hypocapsular mutant, which lacks the *SAC1* gene (*CKF44_06080*). Sac1 is a phosphatase that acts in phosphoinositide (PI) metabolism. Various cellular PI species are defined by the patterns of phosphorylation on their inositol head groups. These species are maintained at distinct cellular compartments by kinases and phosphatases, which specifically and reversibly phosphorylate and dephosphorylate the hydroxyl groups of inositol (27). In this way, PIs help define membrane identity and regulate membrane-protein interactions. By doing so, these lipids play important roles in secretory trafficking (28).

One of the most abundant PI species is phosphatidyl inositol-4-phosphate (PI4P), which is enriched at the trans-Golgi and plasma membrane and modulates late secretory trafficking (29). Dephosphorylation of PI4P is performed by Sac1, a phosphatase that is highly conserved in eukaryotes (30). Our observation that cells lacking Sac1 are hypocapsular suggested that modulation of phosphoinositide turnover in the secretory pathway influences capsule synthesis. Below we

use biochemical, imaging, and molecular engineering approaches to establish the mechanism of this interaction, linking alterations in lipid homeostasis to the production of a critical cryptococcal virulence factor.

RESULTS

Fungal genes that influence interactions with host cells

To identify fungal gene products that affect interactions with host cells, we screened 4,692 *C. neoformans* single gene deletion mutants (20). In our assay, fungal cells were stained with Lucifer Yellow, opsonized with serum, and then incubated with primary mammalian phagocytes to allow engulfment. The samples were then washed to remove unassociated cells, stained with the membrane-impermeant dye Calcofluor White to label externally-associated fungi, fixed, and stained with propidium iodide to label phagocytic cell nuclei. We assessed fungal engulfment as the phagocytic index, or number of internalized fungi (stained with Lucifer Yellow but not Calcofluor White) per host cell (identified by nuclear staining) (24). We define the uptake score as the ratio of a mutant's phagocytic index to that of wild-type *C. neoformans* (KN99).

We first applied our assay to screen the interactions of *C. neoformans* with murine bone marrow-derived macrophages (BMDM), normalizing to fungal cell number to account for differences in mutant growth rates. Because these deletion library plates do not include WT control cells, we initially compared strain uptake scores to the median for each plate and used permissive cutoffs to call roughly 10% of the strains as hits (Table S1A). We then subjected the 458 strains that we identified with increased or decreased uptake (Table S1B) to a second round of BMDM screening (Table S1C), this time comparing them to in-plate wild-type (KN99) controls and using more stringent cutoffs to select hits (Table S1D). In parallel, we screened them using human monocyte-derived macrophages (HMDM) in place of BMDM (Tables S1E and S1F).

Our second round of screening narrowed the initial hits to 93 mutants that significantly influenced host interactions in both BMDM and HMDM cells (Figures 1A-C; Table S1G). When we applied Gene Ontology (GO) analysis to the corresponding genes, we found that cellular factors related to cytoskeletal interactions and intracellular protein localization and transport, among other categories, were enriched in this group relative to their abundance in the genome (Figure 1D; see Discussion).

Mutants with altered host interactions and capsule size

We were particularly interested in identifying gene products that might act in capsule production, because of the many outstanding questions that remain about this process (25). As the outermost layer of the cell, the capsule is fundamental in mediating cryptococcal interactions with host phagocytes (7). Therefore, we hypothesized that the population of strains that showed changes in interactions with phagocytic cells would be enriched for mutants with altered capsule. To test this idea and identify such mutants, we adapted an automated, fluorescence-based capsule quantification assay that we reported earlier (31) to accommodate medium-throughput screening. Of the 458 first round hits from the uptake screen, approximately one third indeed showed capsule changes (Figure 1A), with 57 strains identified as hypocapsular and 74 as hypercapsular (Figure 1E; Tables S2A, 2B). Validating the screen, this group contained multiple strains lacking genes previously shown to influence capsule, including 16 that were hypocapsular and 3 that were hypercapsular. GO term analysis of genes deleted in the hits indicated that they were enriched for gene products related to capsule organization, as we expected, and also for categories related to ion transport, vesicular trafficking, and phosphoinositide binding (Figure 1F; see Discussion).

For further study, we selected 12 of the 131 mutants that showed capsule alterations, based on their potential roles related to secretion and attachment of capsule material. We characterized these strains using phenotypic assays, including plating on media containing specific stressors and growth in mouse lungs (Table S2C). Of this group, we particularly noticed a strain lacking *CKF44_06080*, which showed increased phagocytosis by both BMDM and HMDM and a 61% reduction in capsule thickness compared to WT cells (Figure 2A), as well as temperature sensitivity and increased susceptibility to stress (Table S2C). This sequence encodes a protein with 38% amino acid identity to the phosphatidylinositol phosphatase Sac1 of *Saccharomyces cerevisiae,* including 85% identity across a 20-amino acid region that encodes a conserved $CX_5R(RT)$ motif necessary for catalytic function (32). Interestingly, despite the similarity between the *C. neoformans* and *S. cerevisiae* Sac1 sequences, ectopic overexpression of *S. cerevisiae* Sac1 did not restore the capsule defects of *sac1*Δ cells (Figure S1).

The phenotypes of *sac1*Δ cells, together with the unique biology of the capsule and its importance as a virulence factor, led us to further investigate the role of Sac1 in *C. neoformans*. To pursue these studies, we first engineered a new Sac1 deletion strain (*sac1*Δ) and complemented the mutant at the endogenous site (*SAC1*). We also identified the conserved Sac1 catalytic motif by homology to *S. cerevisiae* Sac1 and inactivated it by replacing an aspartic acid residue with alanine ($SAC1^{456A}$, Figure 2B) (33, 34). Using this strain set, we confirmed that loss of Sac1 leads to increased uptake by

host cells and smaller capsules. Additionally, while complementation restored WT phenotypes, such as normal capsule thickness (Figure 2C, D), the inactivated strain resembled the deletion mutant, showing that the phosphatase function of Sac1 is essential for this biological activity. While imaging, we also observed striking round structures in the *sac1* mutant cells (Figure 2C, right panels). These were distinguished from typical organelles, like the vacuoles visible in WT and *SAC1* cells, by their circular shape, defined edge, and striking refractility and only occurred in *sac1* mutants grown in host-like conditions (here defined as DMEM, 37°C, 5% CO_2). These structures will be further discussed below.

Sac1 is required for cryptococcal virulence

Variations in both uptake and capsule size are associated with changes in pathogenicity (10, 35–41), so we suspected that *sac*1 mutants would have impaired virulence. To test this, we infected mice intranasally and measured organ burden at 14 days post-infection. Notably, while *sac1*Δ cells were recovered from the lungs, they did not exceed the level of the original inoculum. This was in sharp contrast to the lung burden of WT and *SAC1* infected animals, which increased roughly 500-fold in this period (Figure 3). No cells were recovered from the brain in the mutant infections, although time course studies show that WT-infected animals generally have detectable brain burden by this time point (Supp. Figure S2A). We observed similar results with the deletion library *ckf44_06080*Δ strain. This strain demonstrated gradual accumulation of cryptococci in the lung up to 18 days post-infection (Figure S2B) and, like our engineered *sac1* mutant strains, impaired dissemination to the brain (Figure S2C). These results motivated us to define the mechanism(s) by which Sac1 influences virulence.

Sac1 controls substrate distribution and sensitivity to stressors

Sac1 has not been characterized in *C. neoformans.* To test whether it influences the turnover of intracellular PI4P, we engineered strains to express an mNeonGreen-tagged version of a peptide that binds PI4P (FAPP1) and has been used to assess its localization (42). We then examined the abundance and localization of this fluorescent peptide in host-like conditions (Figure 4A). Overall, the FAPP1 signal was brighter in *sac1*Δ cells than in WT, a trend supported by flow cytometry (Figure S3). This is consistent with a role for Sac1 as a PI4P phosphatase, as loss of this protein would lead to an increase in its substrate. We also noted distinctive bright perinuclear rings in the *sac1*Δ cells, which correspond to an endoplasmic reticulum distribution (43). These rings were more diffuse in WT cells. They were particularly notable in rich medium and suggest aberrant accumulation of PI4P in the early secretory pathway. Also absent from WT cells were intense puncta that appeared in the mutant strain and are consistent with PI4P accumulation in the yeast Golgi (44).

Secretion is a vital cellular process, so its perturbation could have multiple deleterious effects on the cell, including effects on the plasma membrane and cell wall. To examine this, we tested strain growth in various stressful conditions. Although both *sac1* mutants grow slightly slower than WT or complemented cells even on rich medium, they showed much worse growth on media containing membrane stressors (the detergent SDS and the sterol binding antifungal drug amphotericin B) or the cell wall stressor Congo Red (Figure 4B). These defects were exacerbated when cells were grown at 37°C. In all of our assays, the complemented strain phenocopied WT and the inactivated construct phenocopied the deletion mutant.

Sac1 regulates cellular lipids during the response to host-like conditions

We sought to explain the capsule defect and stress sensitivities of *sac1* mutants based on the cellular consequences of perturbed PI4P turnover. In other eukaryotes, PI4P is important for establishing the lipid composition of secretory vesicles (45) and its turnover is critical for the progression of post-Golgi secretory traffic (46). We therefore examined classes of molecules, including lipids, proteins, and capsule polysaccharides, that are directly or indirectly influenced by this step of secretion. As noted above, we had observed formation of large internal structures in *sac1* mutant cells grown under host-like conditions (Figure 2C), which were absent from WT and complemented cells. Because of their shape and refractile appearance in light micrographs, we suspected they were at least in part composed of lipid. Consistent with this suggestion, they appeared electron-lucent by transmission electron microscopy (Figure 5A, asterisks). We hypothesized that these structures result from aberrant lipid handling within *sac1* mutant cells that is induced by the stress of host-like conditions, since they are absent from mutant cells grown in rich medium (Figure 5A). Based on this idea, and our results below, we termed them Sac1 lipid-accumulating bodies (SLABs).

SLABs resemble previously-characterized 'supersized lipid droplets' identified in *S. cerevisiae* (47). Lipid droplets are neutral lipid-containing structures that represent essential cellular energy reserves; these increase in abundance when cryptococcal cells are grown in host-like conditions (48). When we stained for neutral lipids using Nile Red, WT cryptococcal cells showed dispersed punctate signal (Figure 5B). In contrast, Nile Red staining of *sac1Δ* cells showed concentrated central staining, frequently colocalized with SLABs (Figure 5B,C), which supported the presence of neutral lipids within them.

We recently demonstrated that mislocalization of the important fungal lipid ergosterol leads to accumulation of neutral lipids in lipid droplets (48). We had also noted that *sac1* mutants were more sensitive than WT cells to the antifungal Amphotericin B, which binds ergosterol (Figure 4B). Considering this information together, we wondered whether

ergosterol localization in *sac1*Δ cells was perturbed. When we stained WT cells grown in host-like conditions with filipin, which binds non-esterified sterols, we saw the typical ring-staining expected for a component of the plasma membrane (Figure 5D). By contrast, mutant cells exhibited increased internal staining, particularly bordering the SLABs (see Discussion).

We fortuitously discovered that supplementation of host-like medium with various exogenous fatty acids restored the growth of *sac1*Δ cells (Supp. Figure S4); this effect is dose-dependent (shown for myristate in Figure 6A). This supplementation also prevented the formation of SLABs (Figure 6B, bottom right panel; see Discussion). When we visualized capsule in myristate-supplemented cells, we made several observations. First, the addition of the BSA vehicle alone led to a capsule size increase, which was of similar magnitude in both cell types. Second, myristate supplementation yielded significant capsule reduction in both strains, which was more dramatic in the mutant (Figure 6B). Lipid supplementation thus restores growth and prevents SLAB formation in *sac1*Δ cells but does not rescue capsule size (see Discussion).

Sac1 impacts protein secretion and localization

Proteins are also critical cargo handled by the secretory pathway, so it is likely that accumulation of PI4P in the secretory pathway would affect their transport and secretion. To assess this, we measured protein secretion directly, using inducible acid phosphatase production as a proxy for general protein secretion (26). Upon entry into phosphate-depleted conditions, WT, *SAC1*, and both *sac1* mutants began producing detectable levels of acid phosphatase within one hour. While the general patterns of secretion were similar, the mutants produced less acid phosphatase on a per cell basis throughout the time course (Figure 7A), suggesting an overall reduction in protein secretion.

Perturbations in PI4P levels may affect not only proteins secreted outside the cell, but also those that reside in the secretory system itself. Importantly, several proteins that participate in cryptococcal capsule synthesis are Golgi-resident. We hypothesized that the loss of PI4P turnover could result in failure to correctly localize these enzymes within the Golgi apparatus and thereby explain the reduced capsule of *sac1* mutants. To investigate this question, we localized the best characterized capsule biosynthetic enzyme, Cxt1 (49), in *sac1*Δ and WT cells grown in host-like conditions. WT cells displayed clear puncta of Cxt1-mNeonGreen, consistent with the expected Golgi localization of this protein. In contrast, staining in *sac1*Δ cells was heterogenous, with various cell populations displaying punctate, diffuse, or little to no fluorescence (Figure 7B, C).

Sac1 affects capsule secretion and composition

Capsule glycans constitute a final class of secretory cargo, which is unique to *C. neoformans*. The predominant capsule polysaccharide, glucuronoxylomannan (GXM), traverses the secretory pathway prior to extracellular release (26). We hypothesized that GXM secretion, like protein secretion, is reduced in *sac1*Δ cells, resulting in their thin capsules. To test this idea, we quantified GXM secretion at intervals after transition to host-like conditions. Importantly, *sac1* mutants began to produce detectable levels of GXM at the same time after induction as WT, indicating that they respond normally to the environmental signals that trigger capsule production (Figure 7D). However, the overall amount of GXM they secreted was markedly reduced.

Reduced GXM secretion could certainly explain the small capsules of *sac1* mutant cells. However, we have observed that features of the capsule, including size and architecture, may also be affected by compositional differences in the polysaccharide itself (9). Mislocalization of glycosyltransferases, such as we observed with Cxt1, could alter the structure of the final capsule polysaccharides. To investigate this idea, we purified GXM from WT, *sac1*Δ, and *SAC1* cells and performed compositional analysis. Compared to the WT and complemented mutant controls, *sac1*Δ GXM showed a substantial (~2-fold) increase in the relative proportion of glucuronic acid, as well as a modest increase in xylose (Figure 7E). These results were supported by linkage analysis, in which we observed a reduction in 3-linked mannopyrannosyl residues as a fraction of the total (Supplemental Table S3), indicating fewer unmodified backbone mannose residues.

DISCUSSION

How *C. neoformans* interacts with host cells is a critical determinant of infection. In this study, we screened 4,692 cryptococcal deletion strains and identified 93 that demonstrated altered uptake by both mouse and human primary phagocytes. GO analysis showed that this set was particularly enriched in sequences that encode proteins with roles in cytoskeletal interactions, protein transport, and organization of the cell wall and capsule. This is consistent with our understanding that the outer layers of the cell and secreted factors are important for modulating interaction with host cells. We also identified strains with defects in only one host system. Why the species differ in this regard could be a fruitful area for future research.

Capsule is a critical factor in the interaction between *C. neoformans* and host cells, but the mechanisms of its synthesis and transport remain largely unknown. To approach this question, we performed a secondary screen for altered capsule thickness, which yielded 131 mutants. For comparison, a previous screen of roughly a quarter as many deletion

library strains, using colony morphology as the primary screen, yielded 16 capsule-related genes (20). Furthermore, our hits represent approximately one third of the original set of uptake mutants that we tested. This shows that our strategy of using these mutants as the starting population to screen for capsule defects was highly successful in enriching for capsule phenotypes. Notably, 42 of the hits are annotated as encoding hypothetical proteins (50) which may be subjects for future investigation. The others were enriched for GO terms related to cell wall and capsule organization, which validated our methods, and for terms involving transporter activity, intracellular transport, and phosphatidylinositol binding. As our results with Sac1 demonstrate, the study of such processes, which are not directly related to capsule production, may still yield insight into capsule biosynthesis.

Interestingly, over half of our capsule screen hits were hypercapsular strains. This highlights an important strength of our image-based technique, as prior methods (including colony morphology, antibody blotting, or volume-based methods) more effectively identify strains that lack capsule (Boodwa-Ko and Doering, in review). That said, image-based screens may also have weaknesses. For example, mutants with general morphological defects may register as false positives, as cells that fail to divide might appear to be one large cell with a capsule defect. Further, this method cannot identify mutants that are completely acapsular, as they will not bind antibody.

Our capsule screen hits were significantly enriched for genes with proposed roles in secretory trafficking (Fig. 1F). As the intracellular movement of capsule material is not well understood, we narrowed our focus to proteins that might be involved in this stage of capsule production. We particularly examined Sac1, a PI4P phosphatase encoded by *CKF44_06080.* The *CNAG_06080* gene (which encodes Sac1 in the closely-related reference strain H99) was previously identified as a site where random integration of a drug marker yielded an attenuated *C. neoformans* strain (51). Like our KN99 mutant, this strain showed reduced virulence, although direct comparison is limited because the mutations, mouse models, and experimental designs differ. Other investigators proposed that this gene was essential, because they were unable to delete it (52). We expect this difference from our findings was due to the challenge of working with cells that have significant defects, although it could also reflect different strain backgrounds (H99S vs KN99) (53, 54).

By expressing and localizing a fluorescent PI4P-binding peptide (42, 55, 56), we supported a role for Sac1 in PI4P turnover in *C. neoformans*. Based on homology to the well-characterized *S. cerevisiae* Sac1 protein, conservation of Sac1 function throughout eukaryotes, and our binding data, we believe PI4P is the main substrate of Sac1 in *C. neoformans*. It

is curious that despite its high amino acid similarity to the *S. cerevisiae* Sac1 protein, over-expression of the latter did not rescue the defects of *C. neoformans sac1*Δ cells; this result may warrant further experimentation.

When s*ac1* mutants are grown in host-like medium, they develop large structures which we term SLABs. The interiors of the SLABs stain with Nile Red, which binds neutral lipids, and the borders stain with the sterol-binding dye filipin. SLABS thus share certain features with lipid droplets, which are composed of a neutral lipid core of mainly triacylglycerols and sterol esters surrounded by a phospholipid monolayer (57). More specifically, SLABs resemble "supersized" lipid droplets, which form in model yeast strains with defects in phospholipid metabolism (47, 58). This phenomenon has also been observed in *C. neoformans* following treatment with the antidepressant sertraline (59). However, our filipin staining suggests the presence of ergosterol or sterol intermediates (60) on the perimeter of the SLABs, which has not been reported for regular or supersized lipid droplets. Ergosterol is distributed in a steep gradient from the ER to the Golgi (61). One model proposes that PI4P turnover by Sac1 maintains this gradient (62). If this mechanism occurs in *C. neoformans,* loss of PI4P turnover would likely result in the inability to shuttle ergosterol up its concentration gradient. Another model suggests that the ergosterol gradient depends on membrane phospholipid composition (61). In either case, loss of Sac1 could perturb lipid transport and homeostasis and lead to mislocalization of ergosterol.

We propose that the lack of PI4P turnover in *sac1* mutants leads to its accumulation in the cryptococcal secretory system. PI4P is an key signaling lipid, serving as a pro-secretory marker and modulating the exit of secretory traffic from the *trans*-Golgi (29, 45, 63). This is consistent with our observations of reduced protein secretion and mislocalization of the Golgi-resident protein Cxt1 in *sac1*Δ cells. The Golgi serves as a central hub for trafficking of both proteins and lipids, and in doing so plays a key role in membrane trafficking and lipid metabolism (64). We hypothesize that SLAB formation in *sac1* mutants represents the failure of lipid trafficking under stressful, nutrient-limited host-like conditions, leading to the accumulation of lipid cargo and/or lipid metabolic precursors. SLAB formation and the poor growth of *sac1*Δ cells is prevented by fatty acid supplementation, which somehow bypasses the defect caused by PI4P accumulation and allows the cells to grow normally. How this occurs will be an interesting question for future research. Importantly, while fatty acid supplementation rescues SLAB formation in *sac1*Δ cells, capsule production is not restored. This key finding shows that the adverse effects of Sac1 loss occur in divergent pathways.

Capsule material is exported in secretory vesicles (26), so defects in anterograde traffic would also impair this process. Beyond reduced GXM secretion, which is consistent with this expectation, we observed alterations in GXM

composition: the mannose backbone had a large increase in glucuronic acid substitution and a slight increase in xylose. We hypothesize that altered localization of capsule biosynthetic enzymes changes their access to nascent capsule material and precursor molecules. It is unknown whether capsule polysaccharides traverse the cell as subunits or extended polymers (65, 66), but in either case increased exposure to biosynthetic enzymes could result in compositional changes such as we observed. Both the reduction of capsule size and changes in composition in *sac1* mutants likely contribute to their increased uptake by host phagocytes.

We identified *C. neoformans* mutants impaired in host interactions with primary cells and assessed the hits for capsule defects. This strategy greatly increased the number of sequences known to influence capsule production, including many previously uncharacterized genes. Analysis of these genes and the corresponding mutants will help us understand the processes required for synthesis of this central virulence factor, as exemplified in this work on Sac1. Importantly, two-thirds of our original uptake hits did not have altered capsule thickness, implicating additional mechanisms in this fundamental host-pathogen interaction. Further studies will be required to determine what leads to the altered uptake of these strains, which may include changes to the cell wall or surface mannoproteins (25) or structural alterations in the capsule that do not impact its thickness.

METHODS

Detailed methods for cell growth, screening, strain engineering, phenotyping assays including virulence studies, and imaging are provided as Supplementary Material. All animal protocols were approved by the Washington University Institutional Animal Care and Use Committee (Protocol #20-0108).

ACKNOWLEDGEMENTS

We thank Nicole Howard and Suhas Bobba for assistance with BMDM isolation and HMDM culture, Todd Fehniger and lab members for providing LRS chambers, Yan Xie for statistical analysis, Wandy Beatty from the Molecular Microbiology Imaging Facility for electron microscopy, and Tim Levine for plasmid sequences. We appreciate the assistance of Jessica Tuck and Alex Caron with phenotypic characterization and microscopy studies. We thank members of the Doering lab for discussions, and in particular Liza Loza, Daphne Boodwa-Ko, Thomas Hurtaux, and Zanetta Chang for comments on the manuscript.

This work was supported by NIH grants AI140979, AI135012, and AI178330 to T.L.D. E.A.G and H.L.C were partially supported by T32 GM007067, and E.A.G. by a Sondra Schlesinger Graduate Fellowship from the Department of Molecular Microbiology, Washington University School of Medicine. The cryptococcal deletion library, developed by the Madhani lab with funding from R01AI100272, was purchased from the Fungal Genetics Stock Center. The Complex Carbohydrate Research Center is supported by the U.S. Department of Energy, Office of Science, Basic Energy Sciences, grant number DE-SC0015662 to Parastoo Azadi.

REFERENCES

1. Denning DW. 2024. Global incidence and mortality of severe fungal disease. Lancet Infect Dis https://doi.org/10.1016/S1473-3099(23)00692-8.

2. Rajasingham R, Govender NP, Jordan A, Loyse A, Shroufi A, Denning DW, Meya DB, Chiller TM, Boulware DR. 2022. The global burden of HIV-associated cryptococcal infection in adults in 2020: a modelling analysis. Lancet Infect Dis 22:1748–1755.

3. Feldmesser M, Kress Y, Novikoff P, Casadevall A. 2000. *Cryptococcus neoformans* is a facultative intracellular pathogen in murine pulmonary infection. Infect Immun 68:4225–4237.

4. Tucker SC, Casadevall A. 2002. Replication of *Cryptococcus neoformans* in macrophages is accompanied by phagosomal permeabilization and accumulation of vesicles containing polysaccharide in the cytoplasm. Proc Natl Acad Sci U S A 99:3165–3170.

5. Del Poeta M. 2004. Role of phagocytosis in the virulence of *Cryptococcus neoformans*. Eukaryot Cell 3:1067–1075.

6. Osterholzer JJ, Surana R, Milam JE, Montano GT, Chen G-H, Sonstein J, Curtis JL, Huffnagle GB, Toews GB, Olszewski MA. 2009. Cryptococcal urease promotes the accumulation of immature dendritic cells and a non-protective T2 immune response within the lung. Am J Pathol 174:932–943.

7. Gaylord EA, Choy HL, Doering TL. 2020. Dangerous liaisons: Interactions of *Cryptococcus neoformans* with host phagocytes. Pathog Basel Switz 9:891.

8. Luberto C, Martinez-Mariño B, Taraskiewicz D, Bolaños B, Chitano P, Toffaletti DL, Cox GM, Perfect JR, Hannun YA, Balish E, Del Poeta M. 2003. Identification of App1 as a regulator of phagocytosis and virulence of *Cryptococcus neoformans*. J Clin Invest 112:1080–1094.

9. Li LX, Rautengarten C, Heazlewood JL, Doering TL. 2018. UDP-glucuronic acid transport is required for virulence of *cryptococcus neoformans*. mBio 9:e02319-17.

10. Santiago-Tirado FH, Peng T, Yang M, Hang HC, Doering TL. 2015. A Single Protein S-acyl Transferase Acts through Diverse Substrates to Determine Cryptococcal Morphology, Stress Tolerance, and Pathogenic Outcome. PLoS Pathog 11.

11. Steenbergen JN, Shuman HA, Casadevall A. 2001. *Cryptococcus neoformans* interactions with amoebae suggest an explanation for its virulence and intracellular pathogenic strategy in macrophages. Proc Natl Acad Sci 98:15245–15250.

12. Mylonakis E, Moreno R, El Khoury JB, Idnurm A, Heitman J, Calderwood SB, Ausubel FM, Diener A. 2005. *Galleria mellonella* as a model system to study *Cryptococcus neoformans* pathogenesis. Infect Immun 73:3842–3850.

13. Mukaremera L, McDonald TR, Nielsen JN, Molenaar CJ, Akampurira A, Schutz C, Taseera K, Muzoora C, Meintjes G, Meya DB, Boulware DR, Nielsen K. 2019. The mouse inhalation model of *Cryptococcus neoformans* infection recapitulates strain virulence in humans and shows that closely related strains can possess differential virulence. Infect Immun 87:e00046-19.

14. Syme RM, Spurrell JCL, Amankwah EK, Green FHY, Mody CH. 2002. Primary dendritic cells phagocytose *Cryptococcus neoformans* via mannose receptors and Fcγ receptor II for presentation to T lymphocytes. Infect Immun 70:5972–5981.

15. Alvarez M, Casadevall A. 2006. Phagosome extrusion and host-cell survival after *Cryptococcus neoformans* phagocytosis by macrophages. Curr Biol 16:2161–2165.

16. Tenor JL, Oehlers SH, Yang JL, Tobin DM, Perfect JR. 2015. Live imaging of host-parasite interactions in a zebrafish infection model reveals cryptococcal determinants of virulence and central nervous system invasion. mBio 6:e01425-15.

17. Srikanta D, Yang M, Williams M, Doering TL. 2011. A Sensitive High-Throughput Assay for Evaluating Host-Pathogen Interactions in *Cryptococcus neoformans* Infection. PLOS ONE 6:e22773.

18. Chun CD, Madhani HD. 2010. Ctr2 links copper homeostasis to polysaccharide capsule formation and phagocytosis inhibition in the human fungal pathogen *Cryptococcus neoformans*. PLOS ONE 5:e12503.

19. Srikanta D, Hole CR, Williams M, Khader SA, Doering TL. 2017. RNA interference screening reveals host CaMK4 as a regulator of cryptococcal uptake and pathogenesis. Infect Immun 85:e00195-17.

20. Liu OW, Chun CD, Chow ED, Chen C, Madhani HD, Noble SM. 2008. Systematic genetic analysis of virulence in the human fungal pathogen *Cryptococcus neoformans*. Cell 135:174–188.

21. Kaur G, Dufour JM. 2012. Cell lines: Valuable tools or useless artifacts. Spermatogenesis 2:1–5.

22. Merly L, Smith SL. 2017. Murine RAW 264.7 cell line as an immune target: are we missing something? Immunopharmacol Immunotoxicol 39:55–58.

23. Pan C, Kumar C, Bohl S, Klingmueller U, Mann M. 2009. Comparative proteomic phenotyping of cell lines and primary cells to assess preservation of cell type-specific functions. Mol Cell Proteomics MCP 8:443–450.

24. Chang AL, Hole CR, Doering TL. 2019. An automated assay to measure phagocytosis of *Cryptococcus neoformans*. Curr Protoc Microbiol 53:e79.

25. Agustinho DP, Miller LC, Li LX, Doering TL. 2018. Peeling the onion: The outer layers of *Cryptococcus neoformans*. Mem Inst Oswaldo Cruz 113:1–8.

26. Yoneda A, Doering TL. 2006. A Eukaryotic Capsular Polysaccharide Is Synthesized Intracellularly and Secreted via Exocytosis. Mol Biol Cell 17:5131–5140.

27. Baba T, Balla T. 2020. Emerging roles of phosphatidylinositol 4-phosphate and phosphatidylinositol 4,5-bisphosphate as regulators of multiple steps in autophagy. J Biochem (Tokyo) 168:329–336.

28. Di Paolo G, De Camilli P. 2006. Phosphoinositides in cell regulation and membrane dynamics. Nature. Nature Publishing Group.

29. Santiago-Tirado FH, Bretscher A. 2011. Membrane-trafficking sorting hubs: cooperation between PI4P and small GTPases at the trans-Golgi network. Trends Cell Biol 21:515–525.

30. Del Bel LM, Brill JA. 2018. Sac1, a lipid phosphatase at the interface of vesicular and nonvesicular transport. Traffic 19:301–318.

31. Reuwsaat JCV, Agustinho DP, Motta H, Chang AL, Brown H, Brent MR, Kmetzsch L, Doering TL. 2021. The transcription factor Pdr802 regulates titan cell formation and pathogenicity of *Cryptococcus neoformans*. mBio 12:e03457-20.

32. Hughes WE, Cooke FT, Parker PJ. 2000. Sac phosphatase domain proteins. Biochem J 350:337–352.

33. Kearns BG, McGee TP, Mayinger P, Gedvilaite A, Phillips SE, Kagiwada S, Bankaitis VA. 1997. Essential role for diacylglycerol in protein transport from the yeast Golgi complex. Nature 387:101–105.

34. Del Bel LM, Griffiths N, Wilk R, Wei H-C, Blagoveshchenskaya A, Burgess J, Polevoy G, Price JV, Mayinger P, Brill JA. 2018. The phosphoinositide phosphatase Sac1 regulates cell shape and microtubule stability in the developing *Drosophila* eye. Dev Camb Engl 145:dev151571.

35. Chang YC, Kwon-Chung KJ. 1994. Complementation of a capsule-deficient mutation of *Cryptococcus neoformans* restores its virulence. Mol Cell Biol 14:4912–4919.

36. Chang YC, Penoyer LA, Kwon-Chung KJ. 1996. The second capsule gene of *Cryptococcus neoformans*, CAP64, is essential for virulence. Infect Immun 64:1977–1983.

37. Chang YC, Kwon-Chung KJ. 1998. Isolation of the third capsule-associated gene, *CAP60*, required for virulence in *Cryptococcus neoformans*. Infect Immun 66:2230–2236.

38. Chang YC, Kwon-Chung KJ. 1999. Isolation, characterization, and localization of a capsule-associated gene, *CAP10*, of *Cryptococcus neoformans*. J Bacteriol 181:5636–5643.

39. Chun CD, Brown JCS, Madhani HD. 2011. A major role for capsule-independent phagocytosis-inhibitory mechanisms in mammalian infection by *Cryptococcus neoformans*. Cell Host Microbe 9:243–251.

40. Bojarczuk A, Miller KA, Hotham R, Lewis A, Ogryzko NV, Kamuyango AA, Frost H, Gibson RH, Stillman E, May RC, Renshaw SA, Johnston SA. 2016. *Cryptococcus neoformans* intracellular proliferation and capsule size determines early macrophage control of infection. Sci Rep 6:1–15.

41. Reuwsaat JCV, Doering TL, Kmetzsch L. 2021. Too much of a good thing: Overproduction of virulence factors impairs cryptococcal pathogenicity. Microb Cell 8:108–110.

42. Levine TP, Munro S. 2002. Targeting of Golgi-specific pleckstrin homology domains involves both PtdIns 4-kinase-dependent and -independent components. Curr Biol CB 12:695–704.

43. Horianopoulos LC, Lee CWJ, Hu G, Caza M, Kronstad JW. 2021. Dnj1 promotes virulence in *Cryptococcus neoformans* by maintaining robust endoplasmic reticulum homeostasis under temperature stress. Front Microbiol 12.

44. Wang ZA, Griffith CL, Skowyra ML, Salinas N, Williams M, Maier EJ, Gish SR, Liu H, Brent MR, Doering TL. 2014. *Cryptococcus neoformans* dual GDP-mannose transporters and their role in biology and virulence. Eukaryot Cell 13:832–842.

45. Johansen J, Ramanathan V, Beh CT. 2012. Vesicle trafficking from a lipid perspective. Cell Logist 2:151–160.

46. Ling Y, Hayano S, Novick P. 2014. Osh4p is needed to reduce the level of phosphatidylinositol-4-phosphate on secretory vesicles as they mature. Mol Biol Cell 25:3389–3400.

47. Fei W, Shui G, Zhang Y, Krahmer N, Ferguson C, Kapterian TS, Lin RC, Dawes IW, Brown AJ, Li P, Huang X, Parton RG, Wenk MR, Walther TC, Yang H. 2011. A role for phosphatidic acid in the formation of "supersized" lipid droplets. PLoS Genet 7.

48. Choy HL, Gaylord EA, Doering TL. 2023. Ergosterol distribution controls surface structure formation and fungal pathogenicity. mBio 14:e01353-23.

49. Klutts JS, Doering TL. 2008. Cryptococcal xylosyltransferase 1 (Cxt1p) from *Cryptococcus neoformans* plays a direct role in the synthesis of capsule polysaccharides. J Biol Chem 283:14327–14334.

50. Basenko EY, Pulman JA, Shanmugasundram A, Harb OS, Crouch K, Starns D, Warrenfeltz S, Aurrecoechea C, Christian J. Stoeckert J, Kissinger JC, Roos DS, Hertz-Fowler C. 2018. FungiDB: an integrated bioinformatic resource for fungi and oomycetes. J Fungi 4.

51. Arras SDM, Chitty JL, Blake KL, Schulz BL, Fraser JA. 2015. A genomic safe haven for mutant complementation in *Cryptococcus neoformans*. PLoS ONE 10:e0122916.

52. Jin J-H, Lee K-T, Hong J, Lee D, Jang E-H, Kim J-Y, Lee Y, Lee S-H, So Y-S, Jung K-W, Lee D-G, Jeong E, Lee M, Jang Y-B, Choi Y, Lee MH, Kim J-S, Yu S-R, Choi J-T, La J-W, Choi H, Kim S-W, Seo KJ, Lee Y, Thak EJ, Choi J, Averette AF, Lee Y-H, Heitman J, Kang HA, Cheong E, Bahn Y-S. 2020. Genome-wide functional analysis of phosphatases in the pathogenic fungus *Cryptococcus neoformans*. 1. Nat Commun 11:4212.

53. Nielsen K, Cox GM, Wang P, Toffaletti DL, Perfect JR, Heitman J. 2003. Sexual cycle of *Cryptococcus neoformans* var. *grubii* and virulence of congenic a and α isolates. Infect Immun 71:4831–4841.

54. Fernandes KE, Fraser JA, Carter DA. 2022. Lineages derived from *Cryptococcus neoformans* type strain H99 support a link between the capacity to be pleomorphic and virulence. mBio 13:e00283-22.

55. Godi A, Campli AD, Konstantakopoulos A, Tullio GD, Alessi DR, Kular GS, Daniele T, Marra P, Lucocq JM, Matteis MAD. 2004. FAPPs control Golgi-to-cell-surface membrane traffic by binding to ARF and PtdIns(4)P. 5. Nat Cell Biol 6:393–404.

56. Dowler S, Currie RA, Campbell DG, Deak M, Kular G, Downes CP, Alessi DR. 2000. Identification of pleckstrin-homology-domain-containing proteins with novel phosphoinositide-binding specificities. Biochem J 351:19–31.

57. Walther TC, Chung J, Farese RV. 2017. Lipid droplet biogenesis. Annu Rev Cell Dev Biol 33:491–510.

58. Fei W, Shui G, Gaeta B, Du X, Kuerschner L, Li P, Brown AJ, Wenk MR, Parton RG, Yang H. 2008. Fld1p, a functional homologue of human seipin, regulates the size of lipid droplets in yeast. J Cell Biol 180:473–482.

59. Breuer MR, Dasgupta A, Vasselli JG, Lin X, Shaw BD, Sachs MS. 2022. The antidepressant sertraline induces the formation of supersized lipid droplets in the human pathogen *Cryptococcus neoformans*. J Fungi 8:642.

60. Solanko KA, Modzel M, Solanko LM, Wüstner D. 2016. Fluorescent sterols and cholesteryl esters as probes for intracellular cholesterol transport. Lipid Insights 8:95–114.

61. Menon AK. 2018. Sterol gradients in cells. Curr Opin Cell Biol 53:37–43.

62. von Filseck JM, Vanni S, Mesmin B, Antonny B, Drin G. 2015. A phosphatidylinositol-4-phosphate powered exchange mechanism to create a lipid gradient between membranes. 1. Nat Commun 6:6671.

63. Santiago-Tirado FH, Legesse-Miller A, Schott D, Bretscher A. 2011. Phosphatidylinositol 4-phosphate and Rab inputs collaborate in myosin-V-dependent transport of secretory compartments in yeast. Dev Cell 20:47–59.

64. Bankaitis VA, Garcia-Mata R, Mousley CJ. 2012. Golgi membrane dynamics viewed through a lens of lipids. Curr Biol CB 22:R414–R424.

65. McFadden DC, Fries BC, Wang F, Casadevall A. 2007. Capsule structural heterogeneity and antigenic variation in *Cryptococcus neoformans*. Eukaryot Cell 6:1464–1473.

66. Doering TL. 2009. How sweet it is! Cell wall biogenesis and polysaccharide capsule formation in *Cryptococcus neoformans*. Annu Rev Microbiol 63:223–247.

67. Chang AL, Kang Y, Doering TL. 2019. Cdk8 and Ssn801 regulate oxidative stress resistance and virulence in *Cryptococcus neoformans*. mBio 10:e02818-18.

68. Ashburner M, Ball CA, Blake JA, Botstein D, Butler H, Cherry JM, Davis AP, Dolinski K, Dwight SS, Eppig JT, Harris MA, Hill DP, Issel-Tarver L, Kasarskis A, Lewis S, Matese JC, Richardson JE, Ringwald M, Rubin GM, Sherlock G. 2000. Gene Ontology: tool for the unification of biology. 1. Nat Genet 25:25–29.

69. The Gene Ontology Consortium, Aleksander SA, Balhoff J, Carbon S, Cherry JM, Drabkin HJ, Ebert D, Feuermann M, Gaudet P, Harris NL, Hill DP, Lee R, Mi H, Moxon S, Mungall CJ, Muruganugan A, Mushayahama T, Sternberg PW, Thomas PD, Van Auken K, Ramsey J, Siegele DA, Chisholm RL, Fey P, Aspromonte MC, Nugnes MV, Quaglia F, Tosatto S, Giglio M, Nadendla S, Antonazzo G, Attrill H, dos Santos G, Marygold S, Strelets V, Tabone CJ, Thurmond J, Zhou P, Ahmed SH, Asanitthong P, Luna Buitrago D, Erdol MN, Gage MC, Ali Kadhum M, Li KYC, Long M, Michalak A, Pesala A, Pritazahra A, Saverimuttu SCC, Su R, Thurlow KE, Lovering RC, Logie C, Oliferenko S, Blake J, Christie K, Corbani L, Dolan ME, Drabkin HJ, Hill DP, Ni L, Sitnikov D, Smith C, Cuzick A, Seager J, Cooper L, Elser J, Jaiswal P, Gupta P, Jaiswal P, Naithani S, Lera-Ramirez M, Rutherford K, Wood V, De Pons JL, Dwinell MR, Hayman GT, Kaldunski ML, Kwitek AE, Laulederkind SJF, Tutaj MA, Vedi M, Wang S-J, D'Eustachio P, Aimo L, Axelsen K, Bridge A, Hyka-Nouspikel N, Morgat A, Aleksander SA, Cherry JM, Engel SR, Karra K, Miyasato SR, Nash RS, Skrzypek MS, Weng S, Wong ED, Bakker E, Berardini TZ, Reiser L, Auchincloss A, Axelsen K, Argoud-Puy G, Blatter M-C, Boutet E, Breuza L, Bridge A, Casals-Casas C, Coudert E, Estreicher A, Livia Famiglietti M, Feuermann M, Gos A, Gruaz-Gumowski N, Hulo C, Hyka-Nouspikel N, Jungo F, Le Mercier P, Lieberherr D, Masson P, Morgat A, Pedruzzi I, Pourcel L, Poux S, Rivoire C, Sundaram S, Bateman A, Bowler-Barnett E, Bye-A-Jee H, Denny P, Ignatchenko A, Ishtiaq R, Lock A, Lussi Y, Magrane M, Martin MJ, Orchard S, Raposo P, Speretta E, Tyagi N, Warner K, Zaru R, Diehl AD, Lee R, Chan J, Diamantakis S, Raciti D, Zarowiecki M, Fisher M, James-Zorn C, Ponferrada V, Zorn A, Ramachandran S, Ruzicka L, Westerfield M. 2023. The Gene Ontology knowledgebase in 2023. Genetics 224:iyad031.

70. Fu J, Hettler E, Wickes BL. 2006. Split marker transformation increases homologous integration frequency in *Cryptococcus neoformans*. Fungal Genet Biol 43:200–212.

71. Thompson JD, Higgins DG, Gibson TJ. 1994. CLUSTAL W: improving the sensitivity of progressive multiple sequence alignment through sequence weighting, position-specific gap penalties and weight matrix choice. Nucleic Acids Res 22:4673–4680.

72. Upadhya R, Lam WC, Maybruck B, Donlin MJ, Chang AL, Kayode S, Ormerod KL, Fraser JA, Doering TL, Lodge JK. 2017. A fluorogenic *C. neoformans* reporter strain with a robust expression of m-cherry expressed from a safe haven site in the genome. Fungal Genet Biol FG B 108:13–25.

73. Huang MY, Joshi MB, Boucher MJ, Lee S, Loza LC, Gaylord EA, Doering TL, Madhani HD. 2022. Short homology-directed repair using optimized Cas9 in the pathogen *Cryptococcus neoformans* enables rapid gene deletion and tagging. Genetics 220:iyab180.

74. Willis LM, Stupak J, Richards MR, Lowary TL, Li J, Whitfield C. 2013. Conserved glycolipid termini in capsular polysaccharides synthesized by ATP-binding cassette transporter-dependent pathways in Gram-negative pathogens. Proc Natl Acad Sci 110:7868–7873.

SUPPLEMENTAL MATERIAL FOR GAYLORD ET AL

Supplemental Methods

BMDM preparation

BMDMs were isolated as in (67) from 9-week old C57BL/6J mice and frozen in 90% FBS, 10% DMSO at 10^7 cells/mL. Thawed cells were differentiated for 9 days in RPMI-1640 with L-glutamine (Sigma) with 30% L-cell supernatant and 20% heat-inactivated fetal bovine serum (Gibco), with regular media changes. BMDM were resuspended in 10 mL ice cold PBS and isolated using 2.5 µg anti-mouse F4/80 biotin (clone BM8, eBiosciences) plus 0.5 µg mouse BD FC-Block (BD Pharmingen) with anti-biotin microbeads (Miltenyi Biotec) and a MACS separation column (Miltenyi Biotec).

Human macrophage preparation

Leukoreduction system (LRS) chambers were obtained from anonymous donors and human peripheral blood mononuclear cells (PMBC) were isolated by Ficoll-Paque centrifugation (Lymphoprep; Axis-Shield). $5x10^7$ PMBC were allowed to adhere to a treated culture dish (Corning) for 2 hours at 37°C with 5% CO_2. Detached cells were removed, and adherent cells were maintained in RPMI-1640 differentiation media containing L-glutamine (Sigma), 10% fetal bovine serum (Sigma), 1% penicillin streptomycin (Fisher), 1% sodium pyruvate (Corning), 50ng/mL human recombinant M-CSF (Fisher), and 1% MEM non-essential amino acids (Corning). Medium was replaced every two days and adherent cells were harvested on day 6 using Cell Stripper (Corning).

Uptake screen

Assays were performed using a modification of our prior method (24). Host cells were seeded in flat clear bottom black polystyrene TC-treated 96-well plates (Corning) at a density of 10^5 cells/well and incubated for one day at 37°C with 5% CO_2. *C. neoformans* strains were cultured from frozen stocks in glycerol/Yeast Extract-Peptone-Dextrose medium (YPD) in 96 well format for 18-24 h at 30°C with shaking (800 rpm) (Southwest Science, SBT1500-H). At least 2 µL of cells were then sub-cultured in 100 µL YPD and grown for 18-24 h as above. After sub-culture, cells were sedimented (3000 g, 2 min, RT), washed twice with 200 µL of PBS, washed once with 200 µL McIlvaine's Buffer [pH 6], and resuspended in 80 µL of the same. Cells were then stained with 5 mg/mL Lucifer Yellow (30 min, RT, 650 rpm) and resuspended in 100 µL of PBS. To account for variation in growth rates of *C. neoformans* mutants, OD_{600} was used to roughly standardize cell number and maintain results in the linear range of the assay. To do this, individual mutants were categorized as having high, medium,

or low growth based on the OD_{600} after resuspension in PBS and the average value of each group was used to prepare wells with approximately 10^7 fungal cells/mL in PBS. Fungal cells were then opsonized with 10% by volume C57Bl6/J mouse serum (for BMDM) or human serum from male AB plasma (for HMDM, Sigma) for 30 minutes at 37°C at 250 rpm. Opsonized cells were then added to wells containing RPMI and macrophages at a multiplicity of infection of 20 (BMDM) or 30 (HMDM). Cells were co-incubated for one hour at 37°C with 5% CO_2 to allow uptake and washed. This and the following washes were performed using a Biotek ELx405 Microplate Washer (2 washes, PBS). Adherent fungal cells were stained with 150 µL of 5 µg/mL Calcofluor White (Sigma) (15 min, 4°C, static). Samples were then washed, fixed with 4% formaldehyde (10 min, RT), washed, permeabilized with 1 mg/mL saponin (20 min, RT), washed, and stained with 50 µg/mL propidium iodide (15 min, RT). Imaging was performed on a BioTek Cytation 3 imager collecting 12 images per well in a 4x3 grid pattern.

A separate plate of each *C. neoformans* strain alone was counted to allow normalization for the number of cells of each mutant strain that were used in the assay. The phagocytic index for each mutant was determined by calculating the number of internalized cells per macrophage and normalizing this to the value for WT KN99 and the number of fungi added. An uptake score was then calculated for each well as fold-change of the normalized phagocytic index compared either to the plate median (for the initial screen of Madhani library plates) or to WT (for the follow-up screens with BMDM and HMDM). For the initial screen of the Madhani deletion collection, we calculated the first quartile (Q1), third quartile (Q3), and interquartile range (IQR) for each plate. We defined hits as those below Q1-c*IQR or above Q3-c*IQR, where c was calculated using a targeted error rate, α, of 0.01. For the second round of screening in BMDM and HMDM, we used an internal WT control and defined hits as those strains whose uptake scores differed from WT in a statistically significant way, using Dunnett's 1-way ANOVA and a p value cutoff of 0.05.

Capsule screen

Strains identified as hits in the uptake assay and wild type control cells were cultured in YPD from frozen stocks in glycerol/YPD in 96 well format (ON, 30 °C, 800 rpm); 10 µL aliquots were then sub-cultured into 190 µL fresh YPD and grown for an additional 24 h. Cells were then sedimented (3000 g, RT) and resuspended in 200 µL DMEM. To achieve the low cell density necessary for optimum capsule induction, the average OD_{600} of the plate was used to calculate the volume of cells to resuspend in 150 µL DMEM to achieve an average OD_{600} of 0.01. Capsule induction was performed in a 96-well glass-bottom plate coated with poly-lysine (Eppendorf) and incubated for 24 h at 37°C with 5% CO_2. KN99α cells grown

overnight in YPD were added to empty wells 10 min before the induction ended to serve as an uninduced control. Following induction, cells were stained and imaged as published previously (31). Briefly, the capsules were stained with anti-capsular monoclonal antibody 302 conjugated to Alexa Fluor 488 (Molecular Probes) and the cell walls stained with Calcofluor White (MP Biomedicals). Imaging was performed on a BioTek Cytation 3 imager collecting 64 images per well in an 8x8 grid pattern. Images were prepared, annotated, and cell wall and capsule diameters for annotated cells calculated as described previously (31). Capsule thickness was defined as the difference between cell wall and capsule diameters. A negative control value (mean capsule thickness of WT cells grown in YPD in the same plate) was subtracted and the result normalized to the value for similarly-corrected positive control samples (WT cells induced in the same plate) to yield a capsule score. Hypocapsular and hypercapsular hits were categorized as those with capsule scores of less than 0.5 or more than 2.0, respectively.

Gene ontology enrichment analysis

Gene ontology (GO) analysis was performed using FungiDB, using both manually curated and computationally predicted GO terms (50, 68, 69). GO categories that were enriched with a P-value cutoff of 0.01 were manually selected for each screen to minimize over-representation of redundant phenotypes.

Strain construction and validation

sac1Δ, *SAC1* complement, and *SAC1*^{D456A} strains were engineered using biolistic transformation with a split-marker strategy (70) in a KN99α background. Design of the catalytically-inactivated construct was based on alignment (71) to the *S. cerevisiae* S288C Sac1 amino acid sequence. mNeonGreen-tagged strains were generated using pBHM2404, a gift from Hiten Madhani (Addgene 173441). PI4P-binding constructs were generated using pRS406-PHO5-GFP-hFAPP1 PH domain, a gift from Tim Levine (Addgene 58723) (42). This sequence was placed between a *TEF1* promoter and terminator and inserted into the Safe Haven 2 (SH2) region of the genome (72). All fluorescent constructs were generated using CRISPR with short homology-directed repair (73). Transformants were confirmed by appropriate antifungal resistance, PCR, and whole genome sequencing.

To test complementation of *sac1*Δ by the corresponding *S. cerevisiae* sequence, the *SAC1* gene was amplified from *S. cerevisiae* strain S288C and inserted into plasmid pMSC042-neo between an *ACT1* promoter and *TRP1* terminator. This construct (containing the promoter, *SAC1* sequence, terminator and antifungal resistance marker) was inserted into the SH2 region of WT and *sac1*Δ cells using CRISPR (72, 73). Total RNA was extracted from cells grown in YPD and DMEM using

TRIzol Reagent (Thermo Fisher) and cDNA was synthesized using the SuperScript III First-Strand Synthesis SuperMix kit (Thermo Fisher). PCR amplification of an S288C Sac1- specific sequence from the cDNA confirmed expression of the S288C *SAC1* gene in both backgrounds (Fig. S1B).

Fungal cell growth and capsule induction

C. neoformans strains were grown from glycerol stocks on YPD plates for 2 days at 30°C. Overnight cultures were inoculated from single colonies into 4 mL of YPD medium and grown overnight at 30°C with shaking (unless otherwise noted). For all capsule induction experiments, overnight cultures were washed in sterile PBS, inoculated into DMEM at 10^6 cells/mL, and grown statically at 37°C with 5% CO_2 for 16-24 hours (as indicated in the text).

Virulence studies

All animal protocols were approved by the Washington University Institutional Animal Care and Use Committee (Protocol #20-0108) and care was taken to minimize animal handling and discomfort. 6-8-week old female C57BL/6 mice (The Jackson Laboratory) were anesthetized by subcutaneous injection of 1.20 mg ketamine and 0.24 mg xylazine in 110 µL sterile PBS. For 14-day infections, mice were intranasally infected with 5×10^4 cryptococcal cells. For time course infection, mice were infected with 1.25×10^4 cryptococcal cells and sacrificed at 6, 12, and 18 days post infection. For both infections, the lungs and brains were harvested, homogenized, and plated on YPD agar for calculation of fungal organ burden.

Stress plate dot spotting

Overnight cultures were pelleted and washed twice in PBS, then diluted to 10^7 cells/mL. 4 µL of this stock and four serial 1:10 dilutions were spotted onto YPD agar and incubated at both 30 and 37°C for 48 hours. To impose plasma membrane stress, the YPD was supplemented with 0.01% sodium dodecyl sulfate or 1 µg/ml amphotericin B; to impose cell wall stress, the YPD was supplemented with 0.05% Congo red.

Acid phosphatase secretion assay

Single colonies were inoculated into 5 mL YPD, grown shaking at 30°C for 6 h, sub-cultured into 25 mL mL MM-KH_2PO_4 (0.5% KH_2PO_4, 15 mM glucose, 10 mM $MgSO_4 \cdot 7H_2O$, 13 mM glycine, 3.0 µM thiamine), and grown overnight at 30°C. Cells were then pelleted, washed twice with MM-KCl (0.5% KCl, 15 mM glucose, 10 mM $MgSO_4 \cdot 7H_2O$, 13 mM glycine, 3.0 µM thiamine), and resuspended in 50 mL MM-KCl at 10^7 cells/mL. Cultures were grown at 30°C with shaking, and 2 mL aliquots were collected at each timepoint. For each, pelleted cells were resuspended in 400 µL substrate buffer (2.5 mM

para-nitrophenylphosphate in 50 mM acetate buffer, pH 4.0, Sigma 71768-5G), incubated at 37°C for 5 minutes, and the reaction stopped with 800 µL saturated Na_2CO_3. Acid phosphatase secretion was quantified using absorbance at 420 nm, corrected by subtraction of a cell-free blank value, and normalized to cell density using OD_{600}.

GXM ELISA

Cultures were induced in DMEM for the indicated times, at which point cells were removed by centrifugation (3000 x g, 5 min, RT), the supernatant fraction filtered through a 0.2µm filter, and the filtrate diluted 1:500 in PBS. Flat-bottom Immulon 1B microtiter plates (Thermo Scientific) were coated overnight with a 1 µg/ml mix of anti-GXM antibodies 339 and F12D2γ in PBS. This and the following incubations were performed at room temperature. The plates were washed twice with 200 µL PBS with 0.5% TWEEN 20 (PBST), blocked for 90 min with 200 µL 1% BSA in PBST. The blocking buffer was replaced with 100 µL PBST and 100 µL of filtered sample was added and incubated for 90 min. The plate was then washed three times as above and the bound GXM was probed with HRP-labeled mAb 339/F12D2γ, incubated for 1 minute with KPL TMB Microwell Peroxidase Substrate (SeraCare), developed, and quantified using absorbance at 450 nm.

Imaging

For fluorescence and confocal microscopy, cells were grown as indicated above and washed twice in PBS. For capsule visualization, cells were resuspended in India ink in PBS (1:2, v:v) and imaged on a ZEISS Axio Imager M2 fluorescence microscope. Capsule thickness was measured manually in ImageJ, using a total of at least 96 cells from at least six randomly-chosen fields of view. To stain neutral lipids, a 0.01% Nile Red stock in acetone was diluted to a working concentration of 0.0005% in PBS. Cells were incubated in 1 mL working Nile Red solution for 15 min in the dark, rotating. Cells were washed twice in PBS, resuspended in PBS, and imaged as above. For quantification of morphology, a minimum of 60 cells from randomly-chosen slide coordinates were examined. For filipin staining, cells were incubated in a freshly prepared solution of 5 µg/mL filipin (Millipore Sigma, F9765-25MG) in DMSO for 15 minutes at room temperature, rotating, then washed twice with PBS before imaging as above. To visualize FAPP1-mNEONGREEN and Cxt1-mNEONGREEN, cells were imaged using a Zeiss LSM880 confocal microscope. For quantification of morphology, a minimum of 94 cells from randomly-chosen slide coordinates were examined. For electron microscopy, cells were grown overnight in YPD or induced for 24 hours in DMEM before processing as in (48), except that the first incubation in 0.1 M sodium cacodylate buffer was performed for 2 h at RT.

Lipid supplementation

For lipid supplementation, a fatty acid stock solution (10 mM in ethanol) was diluted 1:10 into 4 mg/ml BSA in DMEM and then sonicated (Bransonic 2 Ultrasonic Bath Sonicator) before addition to cultures as indicated. After 24-hour of incubation (37°C, 5% CO_2), cells were serially diluted 1:10 and plated onto YPD agar, with the top spot representing the undiluted culture.

GXM purification and analysis

GXM was isolated using selective precipitation of culture supernatants with hexadecyltrimethylammonium bromide (CTAB) as described previously (49). Isolated material was hydrolyzed in trifluoroacetic acid for 3 hours at 100°C and compositional analysis performed using high-performance anion-exchange chromatography with pulsed amperometric detection on a Dionex ICS-6000 instrument (Thermo Scientific). Glycosyl linkage analysis was performed by the Complex Carbohydrate Research Center at the University of Georgia using combined gas chromatography/mass spectrometry of partially methylated alditol acetate derivatives following carboxyl reduction to detect uronic acids (modified from (74)).

Supplemental Table Legends

Supplemental Table S1. Uptake screen results. (S1A) All results from the initial BMDM uptake screen. (S1B) Hits from the initial BMDM uptake screen. (S1C) All results from the second BMDM uptake screen. (S1D) Hits identified from the second BMDM uptake screen. (S1E) All results from the HMDM uptake screen. (S1F) Hits from the HMDM uptake screen.

Supplemental Table S2. Capsule screen results. (S2A) All results from the capsule screen. (S2B) Hits identified from the capsule screen. (S2C) Phenotyping of selected capsule hits.

Supplemental Table S3. Linkage analysis of WT, *sac1*Δ, and *SAC1* strains. Values are the percent area of relevant residue peaks. Numbers in the header row refer to independently isolated samples.

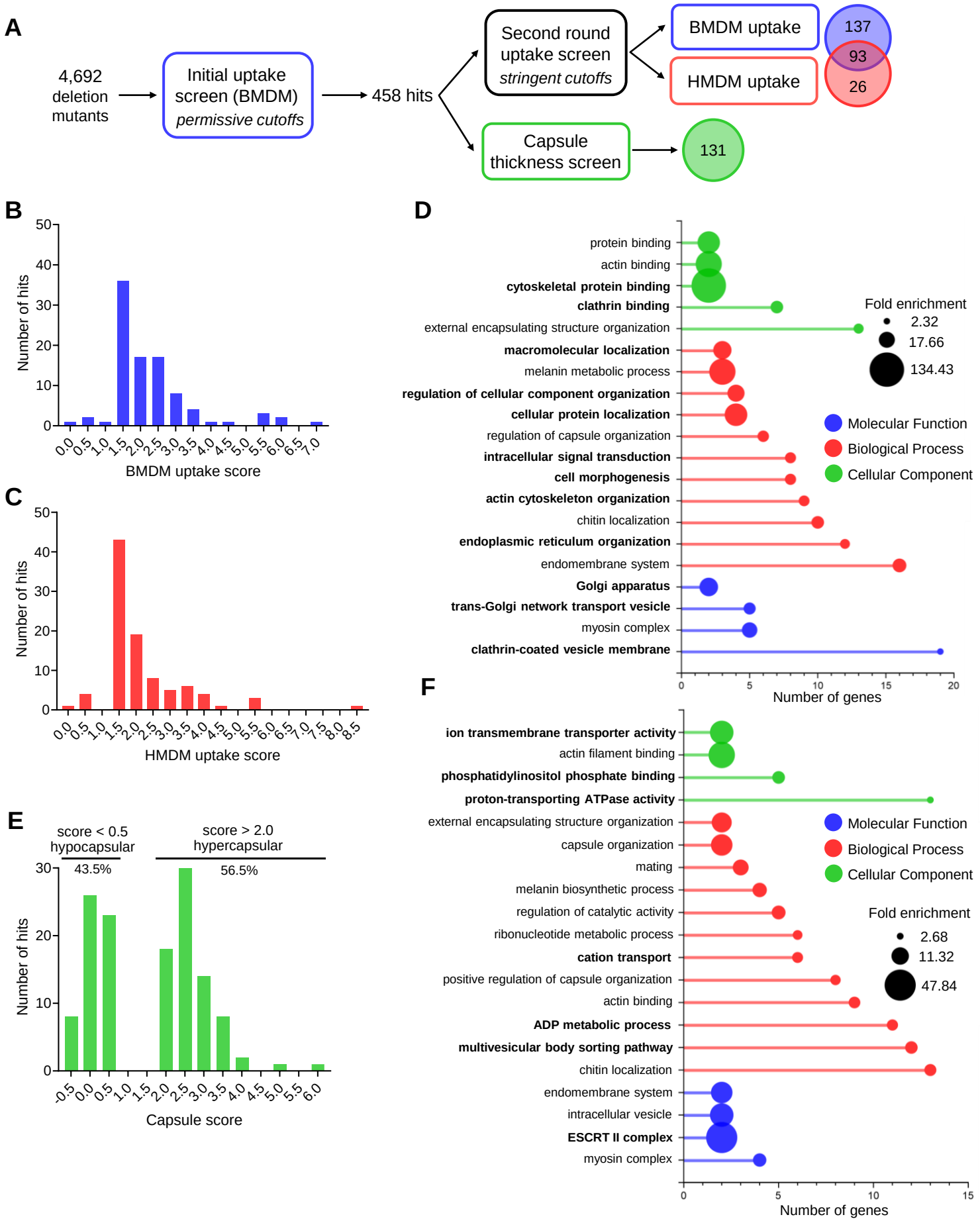

Figure 1. Screen results. (A) Schematic of screening workflow. **(B and C)** Uptake scores (as defined in the text) for the 93 mutants identified as hits when screened against both **(B)** BMDM and **(C)** HMDM. The value under each bar represents the center of the bin and 1.0 is the WT value. **(D)** Selected GO terms that are enriched in the 93 dual hits from the uptake screen. X-axis, number of hit gene IDs which fall within each category. **(E)** Capsule score (capsule thickness relative to that of WT under inducing conditions) for 131 mutants identified as hits in the capsule screen, plotted as in **(B)** and **(C)**. **(F)** Selected GO terms that are enriched in hits from the capsule screen, plotted as in **(D)**. For panels D and F, Bold text denotes categories uniquely enriched for each screen.

A

Deleted gene	Annotation	Uptake score		Normalized capsule size
		BMDM	HMDM	
CKF44_06080	inositol/phosphatidylinositol phosphatase	2.25	1.83	0.39

B

Catalytic motif

*

Sc Sac1 V E I V N E Q H S V V R T N C M D C L D R T N V V Q S **(378-404)**

Cn Sac1 T Q V L T K Q T G V V R T N C M D C L D R T N V A Q A **(440-466)**

C

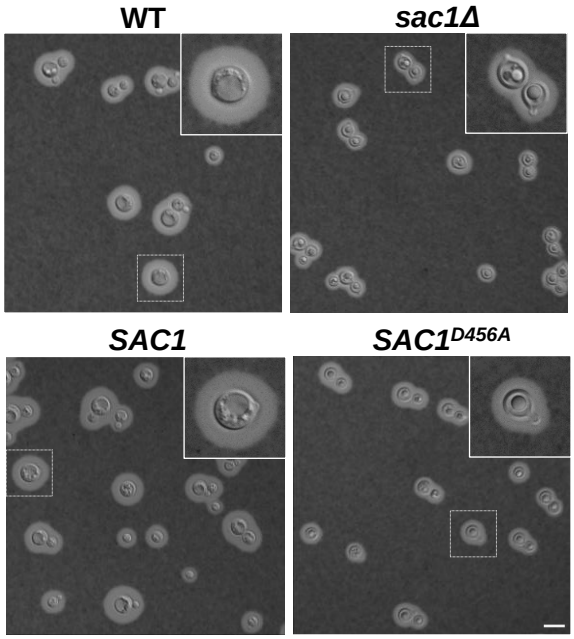

D

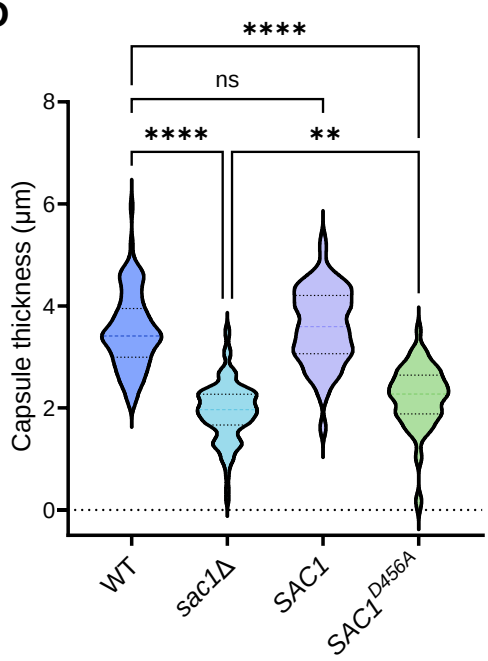

Figure 2. Cells lacking active Sac1 show increased uptake by phagocytes and smaller capsules. (A) Uptake and capsule screen results for cells lacking CKF44_06080. **(B)** Alignment of *C. neoformans* and *S. cerevisiae* sequences that include the Sac1 catalytic motif. Blue, identical residues; asterisk, residue mutated to alanine in the *SAC1^{D456A}* strain. **(C)** India ink negative stain of the indicated strains grown for 24 hours in DMEM at 37°C with 5% CO_2. All primary images are at the same magnification; scale bar, 10 µm. For this and other microscopy figures, any region demarcated by a small square is enlarged in the inset at upper right. **(D)** Distribution of capsule thicknesses for the indicated strains. At least 96 cells were measured for each strain as described in the Methods. **, p<0.0021; ***, p<0.0002; ****, p<0.0001 by 2-way ANOVA with Tukey's multiple comparison test; ns, not significant.

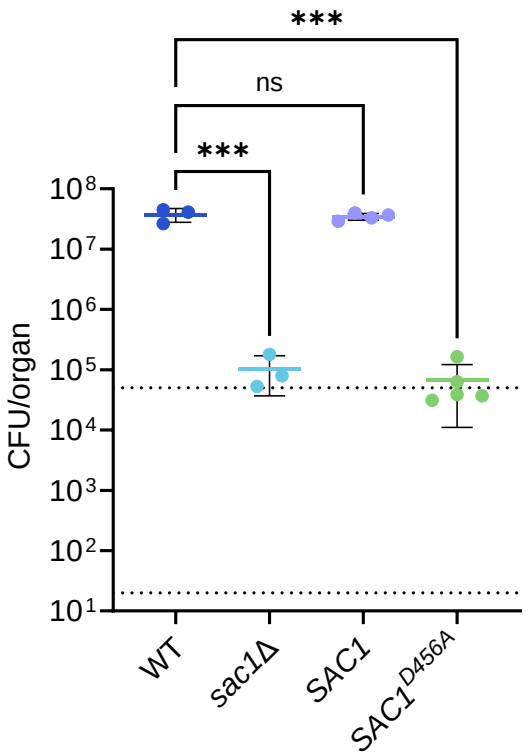

Figure 3. **Sac1 is important for virulence in a mouse infection model.** Lung burden of C57BL/6 mice (groups of 3-5) sacrificed 14 days after intranasal infection with $5x10^4$ fungal cells (upper dotted line). Lower dotted line, limit of detection. Each symbol represents one mouse. ***, $p<0.0002$ by 2-way ANOVA with Tukey's multiple comparison test; ns, not significant.

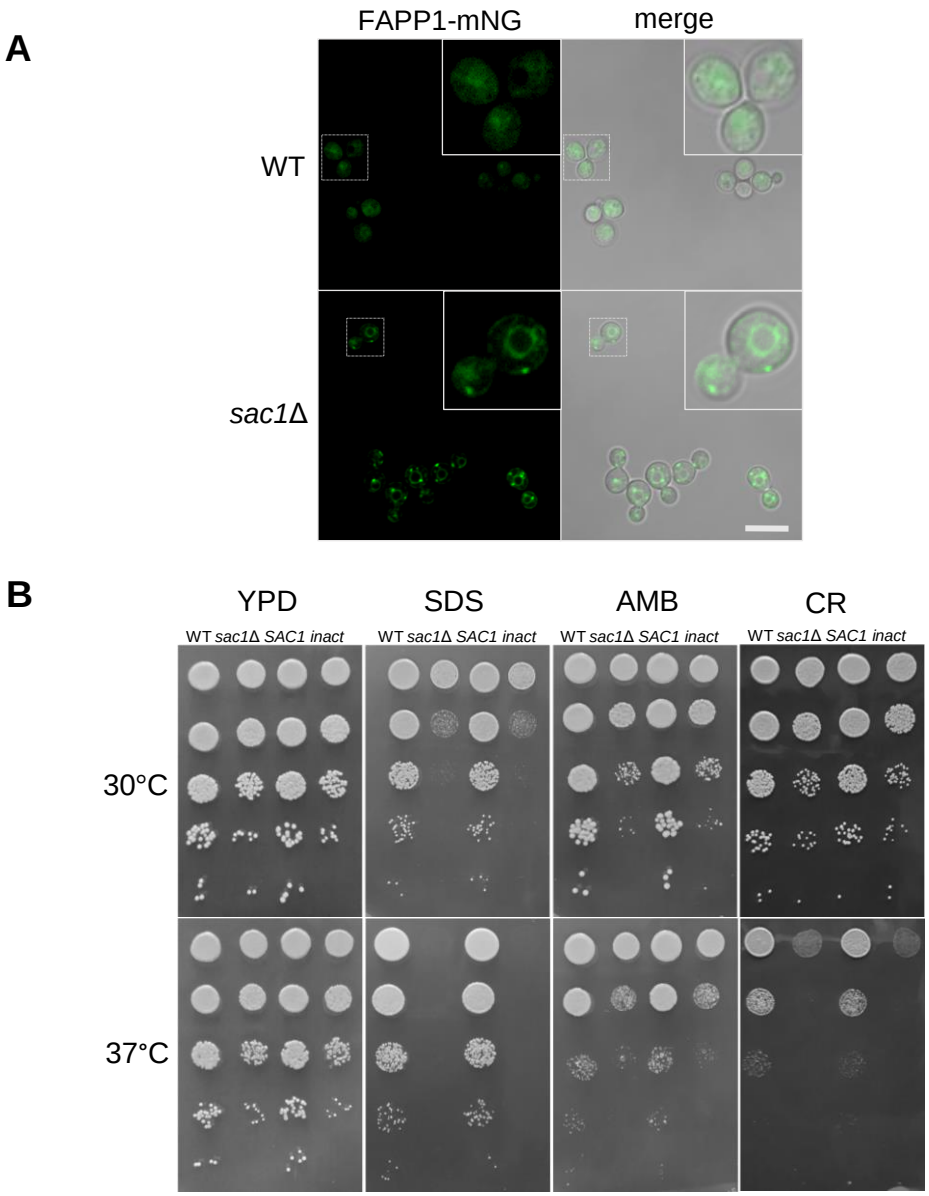

Figure 4. Sac1 regulates substrate distribution and stress sensitivity. (A) FAPP1-mNeonGreen (mNG) localization in cells grown in DMEM at 37°C with 5% CO_2. All primary images are at the same magnification; scale bar, 10 µm. **(B)** Serial 10-fold dilutions of the indicated strains plated on YPD alone or containing 0.01% SDS (SDS), 0.05% Congo Red (CR), or 2 µg/mL Amphotericin B (AMB), incubated at 30 and 37°C. *inact* = *SAC1*^{D456A}.

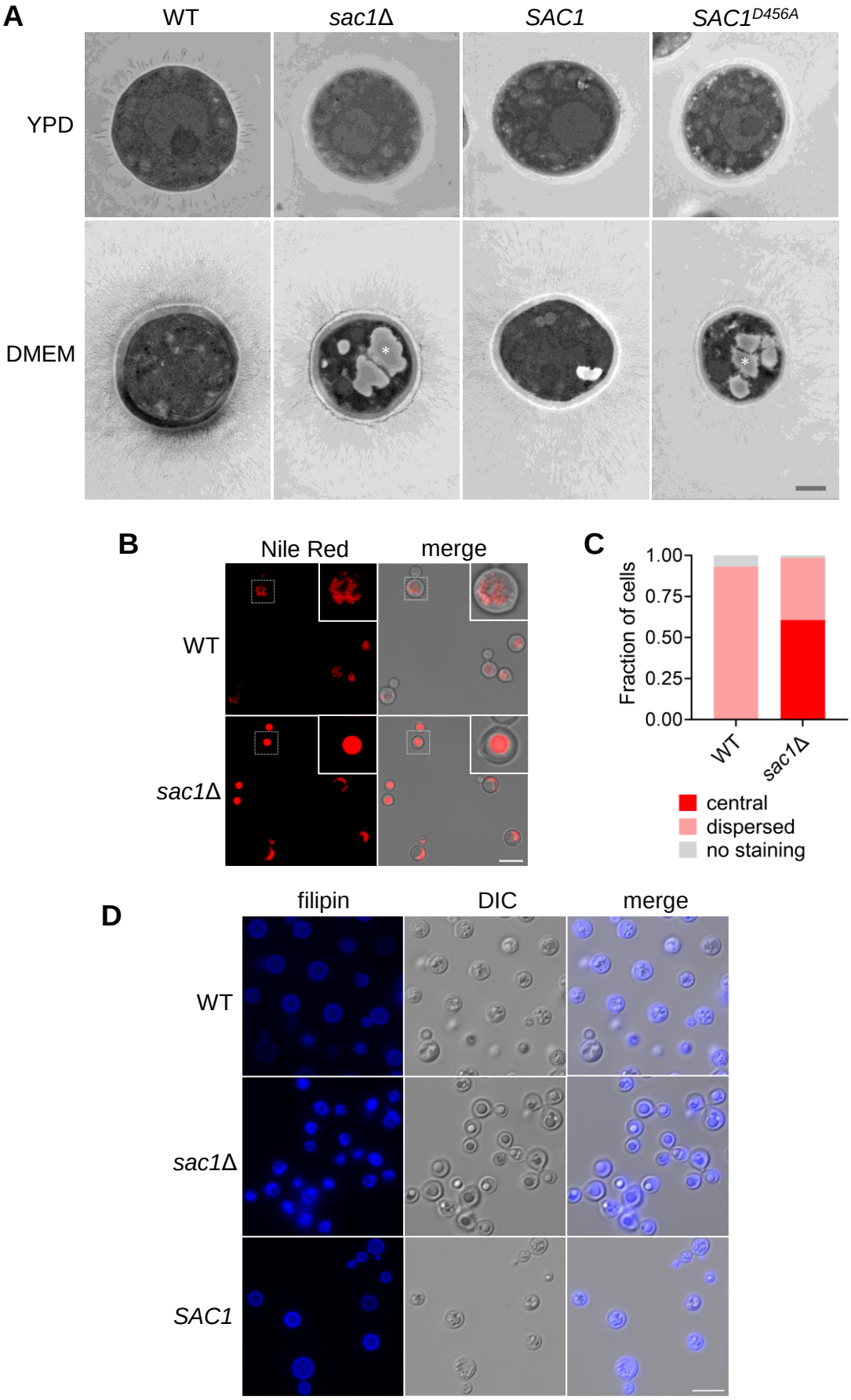

Figure 5. Sac1 is essential for proper lipid trafficking in host-like conditions. (A) Transmission electron micrographs of cells grown in the indicated medium. White asterisks, example lipid droplet structures, likely distorted during sample prep; scale bar, 1 µm. **(B)** Nile Red stain of the indicated strains with **(C)** quantification of the observed staining pattern. **(D)** Filipin staining of cells grown in DMEM. YPD grown cells in Panel A were grown overnight at 30 °C, all other cells were grown for 24 h in DMEM at 37°C with 5% CO_2. Scale bar, 10 µm. All images within each experiment are shown at the same magnification.

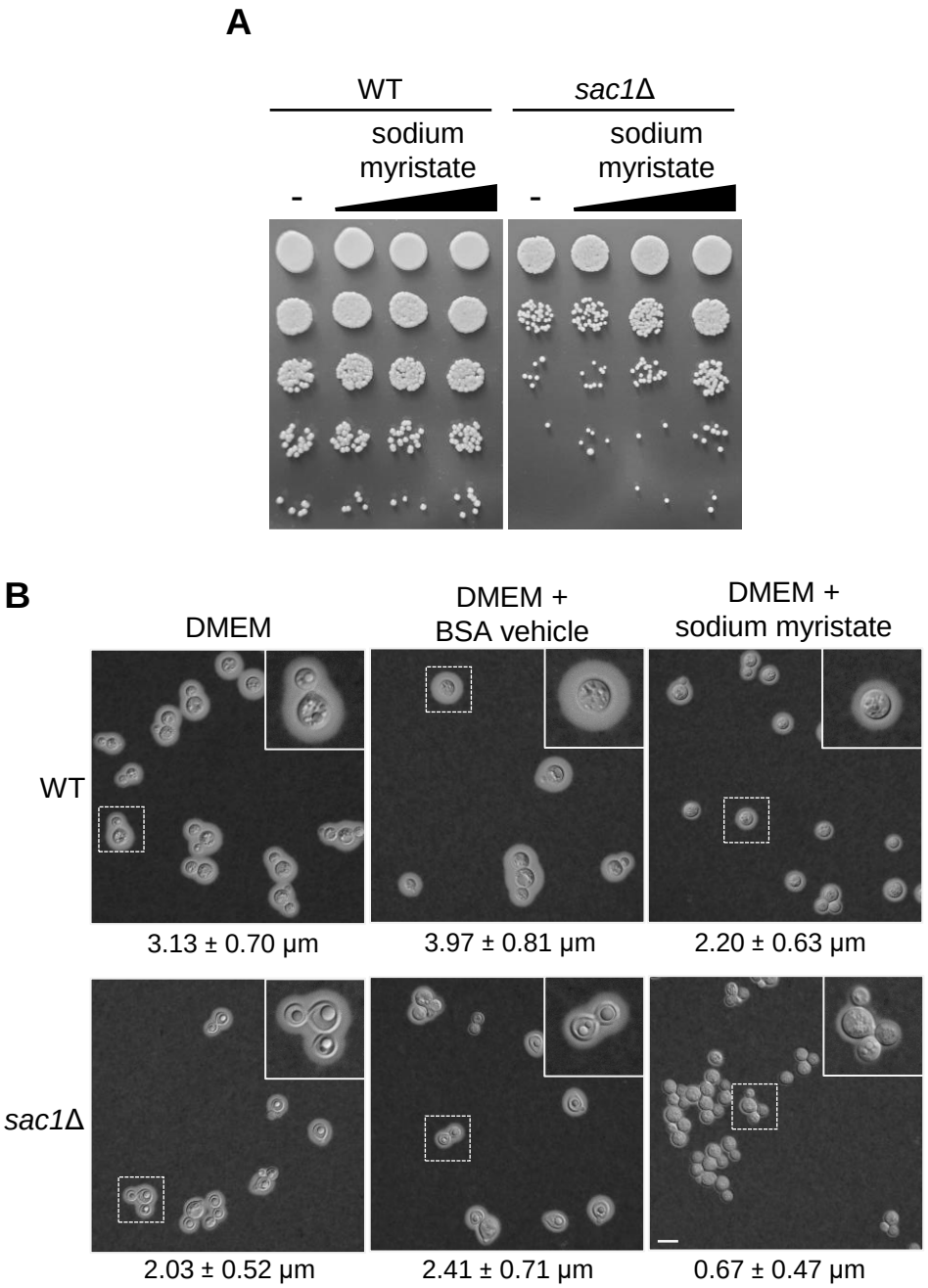

Figure 6. Supplementation with exogenous fatty acid restores *sac1*Δ growth and morphology but not capsule biosynthesis. (A) Serial 10-fold dilutions of WT and *sac1*Δ cells grown for 24 hours in DMEM supplemented with BSA alone (-), or with 8, 40, or 200 µM myristic acid conjugated to BSA (increasing amounts indicated by the triangle). **(B)** India ink negative stain of WT and *sac1*Δ cells grown in DMEM at 37°C with 5% CO_2, supplemented as indicated with BSA alone or 200 µM myristic acid conjugated to BSA. Capsule thickness in µm (mean ± SD) is noted below each panel. All primary images are to the same magnification; scale bar, 10 µm.

.

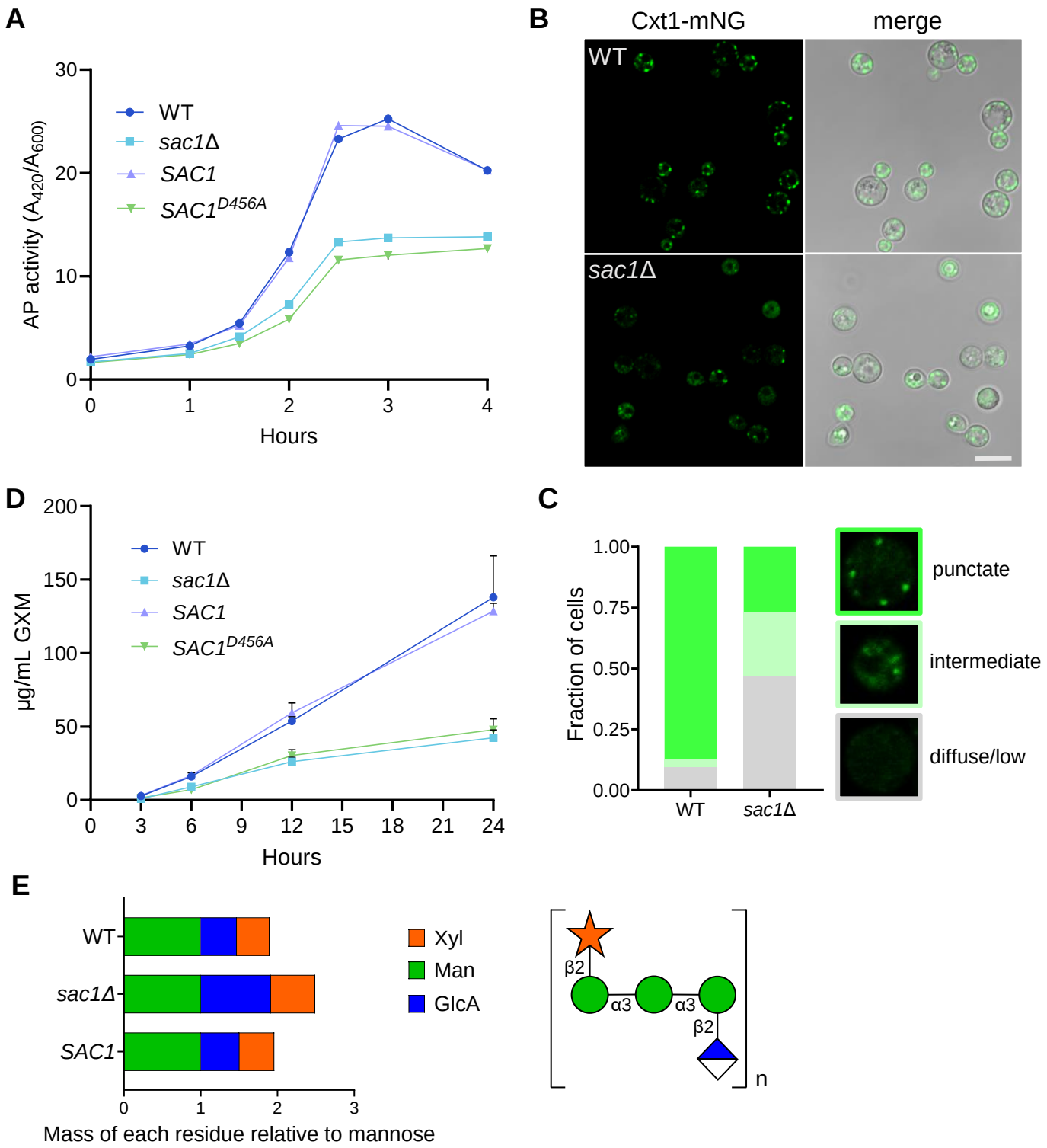

Figure 7. Sac1 controls the secretory pathway to modulate capsule size and composition. (A) Secreted acid phosphatase activity, normalized to cell number, over time after a shift to phosphate-depleted medium. **(B)** Confocal imaging of Cxt1-mNG in the indicated strain backgrounds with **(C)** quantification of observed staining patterns. Punctate: 3 or more puncta present; Intermediate: puncta and diffuse signal; Diffuse/low: diffuse signal or <3 puncta. Images are to the same scale; scale bar, 10 µm. **(D)** Shed GXM quantified by ELISA. For both **(A)** and **(D)**, mean ± SD for one representative experiment of three biological replicate studies is shown. **(E)** Left, GXM composition; right, subunit structure of GXM.

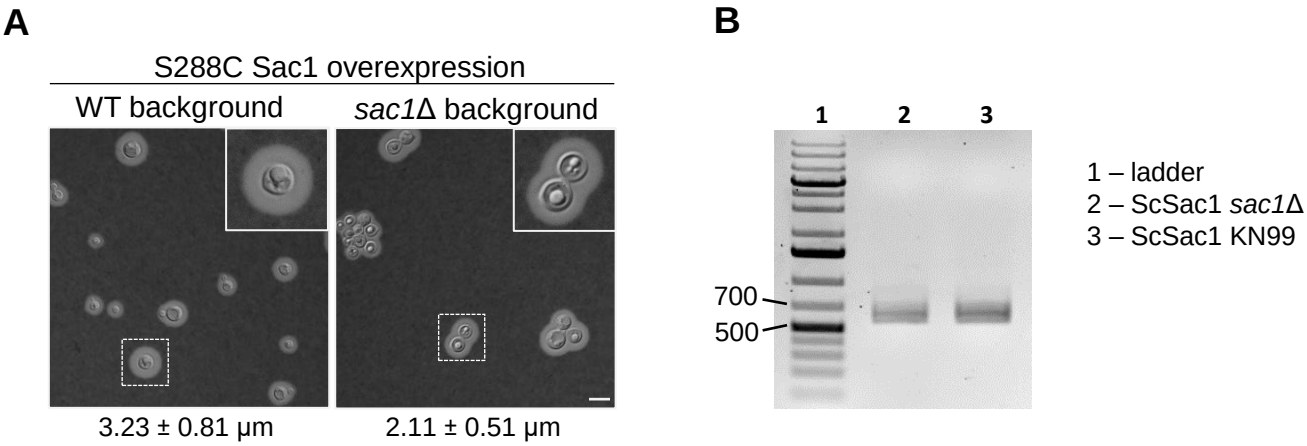

Supplemental Figure S1. Overexpression of the *S. cerevisiae* Sac1 protein in *sac1Δ* does not restore *C. neoformans* capsule synthesis. (A) Negative stain of the indicated strains grown for 24 hours in DMEM at 37°C with 5% CO_2, with the capsule thickness in µm (mean ± SD). Scale bar, 10 µm. **(B)** Amplification of a unique 651 bp region of the S288C Sac1 coding sequence from cDNA generated from fungal cells of the indicated strain grown in YPD shows that the *S. cerevisiae SAC1* gene is expressed in both *C. neoformans* strains.

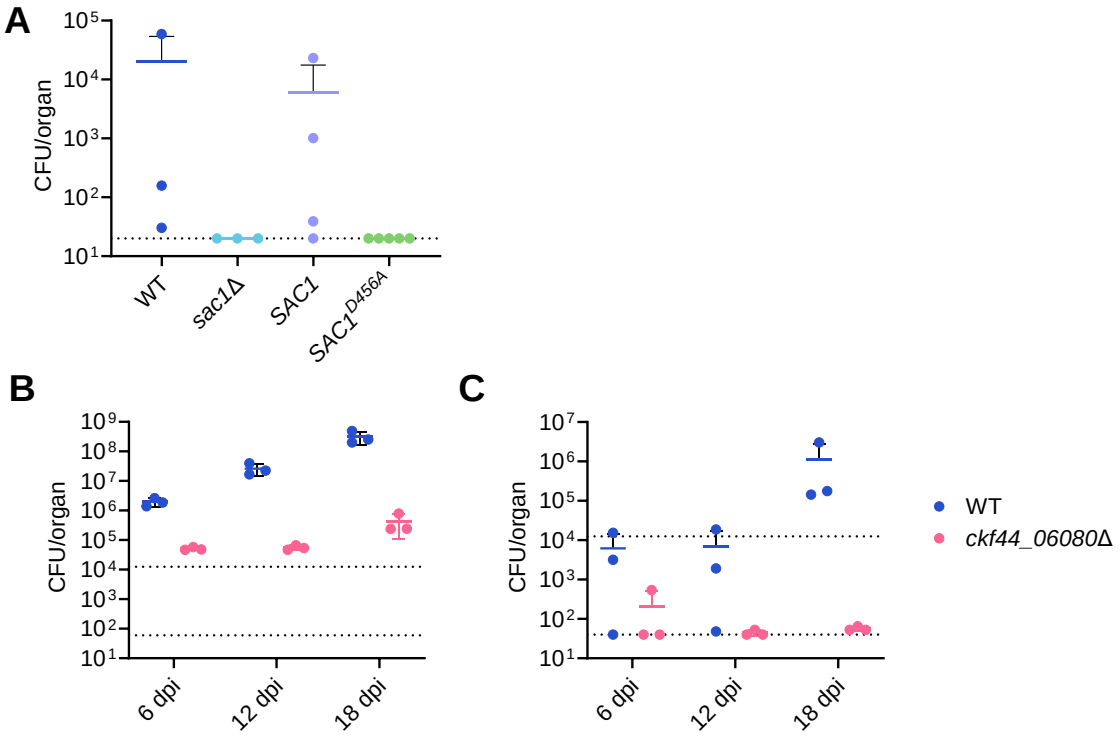

Supplemental Figure S2. Cells lacking functional Sac1 have reduced virulence. Each symbol represents one mouse. **(A)** Brain burden of C57BL/6 mice sacrificed at 14 days post infection with $5x10^4$ fungal cells. Dotted line, limit of detection. **(B)** Lung and **(C)** brain burden of C57BL/6 mice sacrificed at the indicated days post infection (dpi) with $1.25x10^4$ fungal cells. Upper dotted line, inoculum. Lower dotted line, limit of detection.

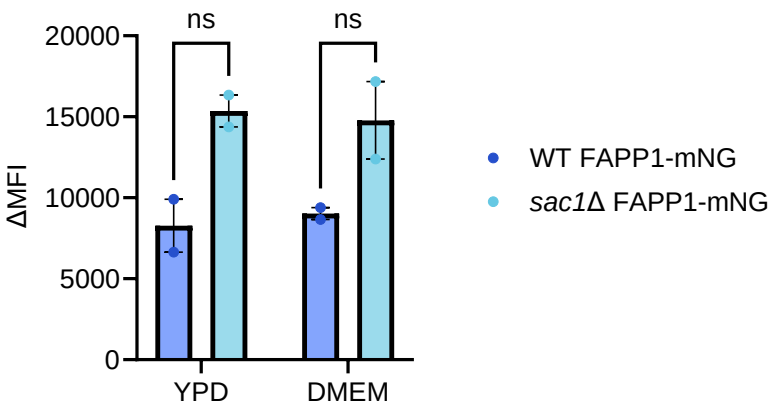

Supplemental Figure S3. PI4P content of WT and *sac1*Δ strains. Difference in median fluorescence intensity between FAPP1-mNG expressing and control cells (ΔMFI) in WT and mutant backgrounds, grown in the indicated medium. ns, not significant by unpaired t test.

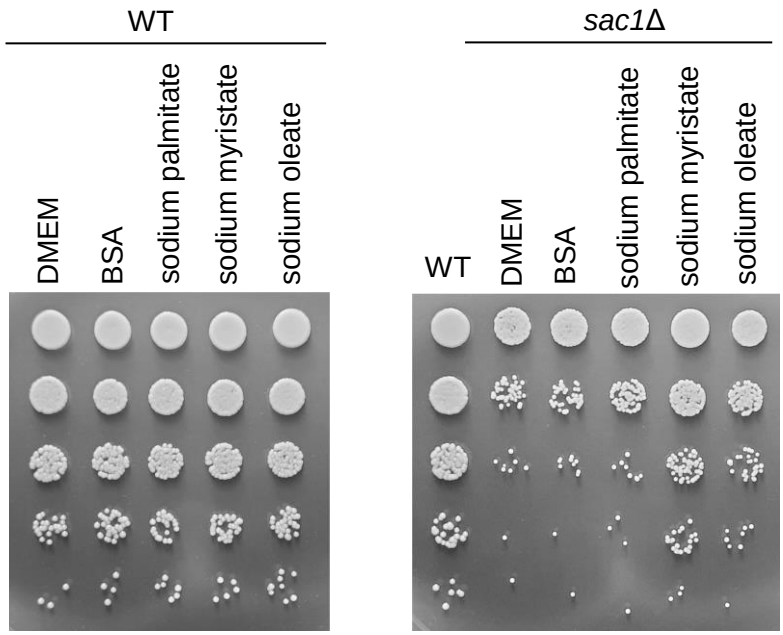

Supplemental Figure S4. Supplementation with exogenous fatty acids restores growth of *sac1*Δ cells. Serial dilutions of (left) WT or (right) *sac1*Δ cells grown for 24 hours in DMEM alone, DMEM supplemented with BSA, or DMEM with 100 μM of the indicated fatty acid sodium salt conjugated to 0.4 mg/mL BSA.

Residue	WT #1	*sac1*Δ #1	WT #2	*sac1*Δ #2	*SAC1* #2
Terminal Xylopyranosyl residue (t-Xyl)	12.0	19.7	10.4	16.2	11.1
Terminal Mannopyranosyl residue (t-Man)	1.3	0.3	0.3	0.3	0.4
Terminal Glucopyranosyl uronic acid residue (t-GlcA)	17.9	15.4	19.1	16.2	18.2
3-linked Mannopyranosyl residue (3-Man)	29.9	23.3	27.8	21.1	30.6
2,3-linked Mannopyranosyl residue (2,3-Man)	36.0	38.5	37.5	42.8	34.9
2,3,4-linked Mannopyranosyl residue (2,3,4-Man)	2.9	2.8	4.9	3.5	4.8

Supplemental Table S3. Linkage analysis of independently isolated WT, sac1Δ, and *SAC1* strains. Values are percent area of relevant residue peaks. Numbers in header row refer to independently isolated samples.